The Astrophysical Journal, 819:121 (8pp), 2016 March 10 doi:10.3847/0004-637X/819/2/121

BROADBAND OBSERVATIONS OF THE GAMMA-RAY EMITTING NARROW LINE SEYFERT 1 GALAXY SBS 0846+513

Vaidehi S. Paliya[1,2], Bhoomika Rajput[1], C. S. Stalin[1], and S. B. Pandey[3]
[1] Indian Institute of Astrophysics, Block II, Koramangala, Bangalore-560034, India; vaidehi@iiap.res.in
[2] Department of Physics, University of Calicut, Malappuram-673635, India
[3] Aryabhatta Research Institute of Observational Sciences, Manora peak, Nainital-263129, India
Received 2015 December 30; accepted 2016 January 16; published 2016 March 7

ABSTRACT

We present the results of our broadband study of the γ-ray emitting narrow line Seyfert 1 (NLSy1) galaxy SBS 0846+513 ($z = 0.585$). This includes multiband flux variations, γ-ray spectral analysis, broadband spectral energy distribution (SED) modeling, and intranight optical variability (INOV) observations carried out over six nights between 2012 November and 2013 March using the 2 m Himalayan *Chandra* Telescope and the 1.3 m telescope at Devasthal, India. Multiple episodes of flaring activity are seen in the γ-ray light curve of the source which are also reflected in the observations at lower frequencies. A statistically significant curvature is noticed in the seven years averaged γ-ray spectrum, thus indicating its similarity with powerful flat spectrum radio quasars (FSRQs). Modeling the SEDs with a one-zone leptonic emission model hints that the optical UV spectrum is dominated by synchrotron radiation, whereas inverse Compton scattering of broad line region photons reproduces the γ-ray part of the SEDs. The source was found to be variable on all the six nights of optical observations with a variation of $\sim$0.3 mag within a single night, coinciding with a high γ-ray activity state. The observed large amplitude INOV clearly indicates the presence of a closely aligned beamed relativistic jet in SBS 0846+513. Our broadband study supports the recent claims in literature that γ-ray emitting NLSy1 galaxies are similar to blazars and constitute the low black hole mass counterparts to FSRQs.

Key words: galaxies: active – galaxies: individual (SBS 0846+513) – galaxies: Seyfert – gamma rays: general

1. INTRODUCTION

The high-energy extragalactic γ-ray sky as seen by the *Fermi* Gamma-ray Space Telescope is dominated by the blazar class of active galactic nuclei (AGNs, e.g., Ackermann et al. 2015). Along with blazars, significant γ-ray emission is also observed from about a half dozen radio-loud narrow line Seyfert 1 (RL-NLSy1) galaxies (e.g., Abdo et al. 2009; Foschini 2011; D'Ammando et al. 2012; Yao et al. 2015). NLSy1 galaxies are a subclass of AGN with peculiar properties that distinguishes them from the conventional broad line Seyfert 1 galaxies. For example, their optical spectra consist of narrow Balmer lines (FWHM (H_β) < 2000 km s^{-1}), weak [O III] ([O III]/H_β<3), and strong optical Fe II lines (Osterbrock & Pogge 1985; Goodrich 1989). They exhibit rapid X-ray flux variations (Pounds et al. 1995) and steep soft X-ray spectra (Boller et al. 1996). It is found that NLSy1 galaxies in general host low-mass black holes ($\sim 10^6 - 10^8\ M_\odot$) accreting close to the Eddington limit (Grupe & Mathur 2004; Xu et al. 2012). About 7% of the NLSy1 galaxy population are found to be radio-loud and many of them exhibit compact core-jet radio morphology, flat/inverted radio spectra, high brightness temperature, and superluminal patterns (Doi et al. 2006; Komossa et al. 2006). These features hint at the presence of closely aligned relativistic jets in them, and observations from the *Fermi*-Large Area Telescope (*Fermi*-LAT) provided confirmation. Therefore, it is of great interest to test their similarities/dissimilarities with the blazar class of AGN, which emits copiously in the γ-ray band. It has been recently reported that the optical and infrared (IR) flux variations of some of these γ-ray emitting NLSy1 (γ-NLSy1) galaxies are similar to blazars (Liu et al. 2010; Jiang et al. 2012; Paliya et al. 2013a). Variable optical polarization similar to that known in several blazars is also observed in some γ-ray emitting NLSy1 galaxies (Itoh et al. 2013, 2014). Blazars are known to show hour-scale γ-ray flux variations (e.g., Foschini et al. 2011) and a similar short timescale γ-ray variability was noticed from a NLSy1 galaxy 1H 0323+342 ($z = 0.063$) during its 2013 September outburst (Paliya et al. 2014). A statistically significant curvature is observed in the γ-ray spectra of few γ-NLSy1 galaxies (Paliya et al. 2015), which indicates their resemblance more to the FSRQ class of blazars. The broadband spectral energy distributions (SEDs) of γ-NLSy1 galaxies exhibit the typical double hump structure (e.g., Abdo et al. 2009; D'Ammando et al. 2012; Paliya et al. 2013b), similar to blazars. Additionally, the requirement of the external Compton (EC) mechanism to explain the γ-ray window of the SED provides more supporting evidence of their resemblance with FSRQs (e.g., Abdo et al. 2009; D'Ammando et al. 2012; Foschini et al. 2012; Paliya et al. 2013b).

SBS 0846+513 (R.A. = 08:49:58.0, J2000; decl. = +51:08:28, J2000; $z = 0.585$) is a NLSy1 galaxy found to be a γ-ray emitter by Foschini (2011). *Fermi*-LAT has observed more than one episodes of γ-ray flaring activity from this object where the isotropic γ-ray luminosity reaches as high as 10^{48} erg s^{-1} (e.g., D'Ammando et al. 2012). Maune et al. (2014) have reported a high-amplitude three-magnitude optical flare in 2013 April that was closely associated with a high γ-ray state. They also reported the detection of high optical polarization ($\sim$10%) during the same period. The very high brightness temperature ($T_b > 10^{13}$ K; Zhou et al. 2005), large amplitude optical variability, and the detection of superluminal motion (D'Ammando et al. 2012) further hint at the presence of a closely aligned relativistic jet in this source. In this work we use all of the publicly available multi-wavelength data taken during the first seven years of *Fermi* operation and study this source in detail. New observations of its intranight-night optical

variability (INOV) characteristics are also presented. Considering a leptonic origin of radiation, we present a consistent picture of the physical properties of this source.

The paper is organized as follows. We describe the adopted data reduction procedure in Section 2. The obtained results are presented and discussed in Section 3 followed by the conclusion in Section 4. We use the cosmological parameters $\Omega_m = 0.27$ and Hubble constant $H_0 = 71\,\mathrm{km\,s^{-1}\,Mpc^{-1}}$.

2. MULTI-WAVELENGTH OBSERVATIONS AND DATA REDUCTIONS

2.1. Fermi-Large Area Telescope Observations

We analyze LAT observations of SBS 0846+513 covering the first seven years of *Fermi* monitoring, i.e., MJD 54683 −57222. We follow the standard data reduction procedure as described in the online documentation[4] and briefly mention it here. We use the latest data set (Pass 8) and in the energy range of 0.1−300 GeV, events belonging to `evclass` 128 and `evtype` 3 and lying within 15° source region are considered. Data analysis is performed with the package `ScienceTools v10r0p5` along with the use of instrument response functions P8R2_SOURCE_V6. To avoid the contamination from Earth limb γ-rays, the maximum zenith angle is set as 90°. The region of interest (ROI) is defined as a circle of 10° radius centered at the γ-ray position of SBS 0846+513, as defined in the third catalog of *Fermi*-LAT detected objects (3FGL; Acero et al. 2015). A maximum likelihood test statistics $(\mathrm{TS}) = 2\Delta \log(\mathcal{L})$, where $\mathcal{L}$ represents the likelihood function between models with and without a point source at the source position, is derived to determine the significance of the γ-ray signal. All the sources present within ROI and defined in the 3FGL catalog are considered for the spectral analysis with their parameters left free to vary during the fitting. In addition, objects lying between 10° and 15° from the source of interest are also included, however their parameters are kept fixed to the 3FGL catalog values. Galactic and the isotropic extragalactic background emissions are also properly accounted for through the use of the latest background templates (`gll_iem_v06.fit` and iso_P8R2_SOURCE_V6_v06.txt, respectively). A binned likelihood analysis is performed over the period of interest and all the sources with $\mathrm{TS} < 25$ are removed. This updated model is then used for further temporal and spectral studies.

All the errors associated with the LAT data analysis are 1σ statistical uncertainties, unless specified. Primarily governed by the uncertainty in the effective area, the systematic uncertainties on the measured fluxes are energy dependent: it amounts to 10% at 30 MeV, decreasing linearly as a function of $\log(E)$ to 3% at 100 MeV, and increases linearly as a function of $\log(E)$ beyond 100 GeV to about 15% at 1 TeV.[5]

2.2. Swift Telescope Observations

The *Swift* telescope (Gehrels et al. 2004) has observed SBS 0846+513 for a total of 14 times in the first seven years of *Fermi* mission (covering MJD 54683−57222 or 2008 August 4 to 2015 July 15). The source was observed by all of the three instruments on board: the Burst Alert Telescope (BAT; Barthelmy et al. 2005, 15–150 keV), the X-Ray Telescope (XRT; Burrows et al. 2005, 0.3−10 keV), and the Ultraviolet/Optical Telescope (UVOT; Roming et al. 2005, 170−600 nm).

SBS 0846+513 is never detected by BAT, primarily due to the poor sensitivity of the instrument for short exposures and because of the low level of hard X-ray emission from the source. Consequently, it is not included in the 70-month *Swift*-BAT hard X-ray catalog (Baumgartner et al. 2013).

We analyze the XRT data following standard procedures available within the HEASOFT package (6.17) and through use of the latest CALDB files. In particular, the tool `xrtpipeline(v.0.13.1)` is used to perform standard screening and filtering criteria on the data set. All XRT observations were taken in the most sensitive photon counting mode and we used the standard grade selection of 0−12. The calibrated and cleaned event files are summed to generate energy spectra. The source spectra are extracted from a circular region centered at the source and having a radii of 47″, whereas the background events are selected from an annular region centered at the source position and have inner and outer radii of 55″ and 110″, respectively. We combined the exposure maps using the tool XIMAGE and ancillary response files are created with `xrtmkarf` to account for vignetting and point-spread function corrections. Due to low photon statistics, we rebinned the spectra to ensure a minimum of one count per bin and used Cash statistics (Cash 1979) to perform spectral analysis. An absorbed power law (PL) (neutral hydrogen column density $N^{\mathrm{H}} = 2.91 \times 10^{20}\,\mathrm{cm^{-2}}$; Kalberla et al. 2005) model is used to perform the fitting within XSPEC (Arnaud 1996).

The observations from Swift UVOT are integrated using the task `uvotimsum`. Source counts are extracted from a 5″ circular region centered on the target and a background is extracted from a larger area free from source contamination. The source magnitudes are extracted with the task `uvotsource`. Observed magnitudes are then de-reddened for galactic extinction (Schlafly & Finkbeiner 2011). The conversion from corrected magnitudes to flux units is done using the zero points and conversion factors of (Breeveld et al. 2011).

2.3. Optical Monitoring Observations

The γ-NLSy1 galaxy SBS 0846+513 was observed on a total of six nights between 2012 November and 2013 March is part of our ongoing campaign on NLSy1 galaxies. Three nights of observations were carried out using the 1.3 m telescope located at Devasthal and operated by the Aryabhatta Research Institute of Observational Sciences (ARIES), India. Three additional nights of monitoring were done using the 2 m Himalayan *Chandra* Telescope at the Indian Astronomical Observatory in Hanle, India. All of the observations were taken in *R* band. We follow the standard procedures in `IRAF`[6] to perform pre-processing of the images (e.g., bias subtraction, flat-fielding, and cosmic ray removal). The instrumental magnitudes of the target and comparison stars in the image frames are determined by aperture photometry using the `phot` task in the APPHOT package in `IRAF`. Following the procedures outlined in Stalin et al. (2004), we derived the optimum aperture radius for photometry. First, we generate star −star differential light curves for a series of aperture radii starting from the median seen at full width at half maximum

[4] http://fermi.gsfc.nasa.gov/ssc/data/analysis/documentation/

[5] http://fermi.gsfc.nasa.gov/ssc/data/analysis/LAT_caveats.html

[6] `IRAF` is distributed by the National Optical Astronomy Observatories, which is operated by the Association of Universities for Research in Astronomy, Inc. under cooperative agreement with the National Science Foundation.

Table 1
Positions and Apparent Magnitudes of the Comparison Stars from the USNO Catalog

Star	R.A. (J2000) (h m s)	Decl. (J2000) (d m s)	R (mag)
S1	08:49:38.49	+51:07:55.52	16.90
S2	08:49:41.34	+51:10:57.97	16.90
S3	08:50:16.73	+51:09:23.36	17.40

(FWHM) that night. The aperture that corresponds to the minimum scatter for the different pairs of comparison stars is selected as the optimum aperture for the photometry of the source. The positions and apparent magnitudes of the comparison stars (taken from USNO[7]) used in the differential photometry are provided in Table 1. It should be noted that uncertainty in the magnitudes taken from this catalog may be up to 0.25 mag (Monet et al. 2003).

3. RESULTS AND DISCUSSION

3.1. Average γ-ray spectra

The seven years averaged *Fermi*-LAT data of SBS 0846+513 is fitted with both PL and log parabola (LP) models and the obtained results are presented in Table 2. As can be seen, the fitting of the PL model indicates a relatively harder γ-ray spectrum of SBS 0846+513 ($\Gamma_{0.1-300\ \mathrm{GeV}} = 2.23 \pm 0.03$) compared with other γ-NLSy1 galaxies (Paliya et al. 2015). The ~7 years average γ-ray flux is $(3.79 \pm 0.16) \times 10^{-8}$ ph cm^{-2} s^{-1} and this corresponds to an isotropic γ-ray luminosity (L_γ) of $\sim 4 \times 10^{46}$ erg s^{-1}. Such a high L_γ is typically observed from FSRQs (e.g., Ackermann et al. 2015). The associated significance of detection is $\sim 50\sigma$ (TS $\approx$ 2635). Moreover, fitting of the LP model hints for the presence of curvature in the γ-ray spectrum ($\beta = 0.11 \pm 0.02$, TS $\approx$ 2650). In general, powerful FSRQs exhibit a curved γ-ray spectrum (e.g., Acero et al. 2015) and this indicates the similarity of SBS 0846+513 with FSRQs.

3.2. Multi-wavelength temporal properties

The long-term multi-wavelength temporal behavior of SBS 0846+513 is presented in Figure 1. In this plot, the *Fermi*-LAT data points are weekly binned and *Swift* observations are shown as one point per observation Id. Multiple episodes of γ-ray flares are visible and it appears from the available observations that the object brightened at other frequencies also is during the period of high γ-ray activity, although it could not be statistically established due to sparseness of the data. The details of these γ-ray flaring behaviors are already described in (Paliya et al. 2015) and here we concentrate more on the multi-frequency properties of SBS 0846+513. From the multi-wavelength light curves, we select two high-activity periods (F1 and F2) and a quiescent period (Q) for further analysis and SED modeling. The choice of the selected periods is driven by the availability of multi-frequency data. As can be seen in Figure 1, observations at lower frequencies are not available during the first flare of SBS 0846+513 (before MJD 55800), and thus this flaring period is not considered for SED analysis. On the other hand, flares during the periods F1 and F2 are simultaneously observed by *Swift*, thus providing an unique opportunity to study them in detail. Interestingly, visual inspection of Figure 1 suggests that the amplitude of γ-ray variability during the periods F1 and F2 seems similar; however, the source appeared brighter during the later period in low frequency *Swift* observations.

[7] http://www.nofs.navy.mil/data/fchpix/

Table 2
Seven Years Averaged LAT Data Analysis of γ-NLSy1 Galaxy SBS 0846+513

Model (1)	$F_{0.1-300}$ GeV (2)	$\Gamma_{0.1-300}/\alpha$ (3)	β (4)	TS (5)	L_γ (6)
PL	3.79 ± 0.16	2.23 ± 0.03	⋯	2634.82	4.25
LP	3.18 ± 0.19	1.96 ± 0.06	0.11 ± 0.02	2648.15	4.30

Note. Column information are as follows: (1) Model used for fitting (PL: power law, LP: log parabola); (2) 0.1−300 GeV flux in units of 10^{-8} ph cm^{-2} s^{-1}; (3) power law photon index or log parabolic photon index at pivot energy obtained from fitting the log parabola model; (4) curvature index; (5) TS; and (6) γ-ray luminosity in units of 10^{46} erg s^{-1}.

3.3. Spectral energy distribution

We generate SEDs for all three periods under consideration (Figure 1) by averaging the fluxes over each time interval. In Table 3 we present the associated flux values obtained from this analysis. We model the SEDs by adopting a one-zone leptonic emission model as described in Ghisellini & Tavecchio (2009) and Dermer et al. (2009) and briefly describe it here. The emission region is assumed to be spherical, moving relativistically with the bulk Lorentz factor Γ at a distance $R_{\rm diss}$ from the central black hole of mass $M_{\rm BH}$. The semi-opening angle of the conical jet is considered as 0.1 rad and the size of the emission region is constrained by assuming it to cover the entire cross-section of the jet. The emission region is filled with the electrons following a smoothly joining broken PL of the form

$$N'(\gamma') = N'_0 \frac{(\gamma'_{\rm brk})^{-p}}{(\gamma'/\gamma'_{\rm brk})^p + (\gamma'/\gamma'_{\rm brk})^q} \quad (1)$$

where p and q are the energy indices before and after the break energy ($\gamma'_{\rm brk}$), respectively (primed quantities are measured in the comoving frame). The accretion disk radiation is modeled by assuming a standard optically thick, geometrically thin Shakura & Sunyaev (1973) disk. Locally its spectrum is assumed as that emitted by a multi-temperature annular blackbody. The broad line region (BLR) is considered as a spherical shell reprocessing 10% of the disk luminosity and emits like a blackbody peaking at the rest-frame Lyα frequency (Tavecchio & Ghisellini 2008). The size of the BLR is assumed to follow the relation $R_{\rm BLR} = 10^{17} L_{\rm disk,45}^{1/2}$ cm, where $L_{\rm disk,45}$ is the accretion disk luminosity in units of 10^{45} erg s^{-1} (Ghisellini & Tavecchio 2009). In our model the presence of the dusty torus is also considered which reprocesses 50% of the accretion disk emission at IR frequencies. For simplicity it is assumed to be a thin spherical shell and its emission is considered as a simple blackbody peaking at the temperature $T_{\rm IR}$. The size of the torus, similar to BLR, scales with the square root of the disk luminosity and assumed to follow the relation $R_{\rm IR} = 10^{18} L_{\rm d,45}^{1/2}$ cm. In the comoving frame, the radiation energy densities of all the components are computed at the distance $R_{\rm diss}$ from the

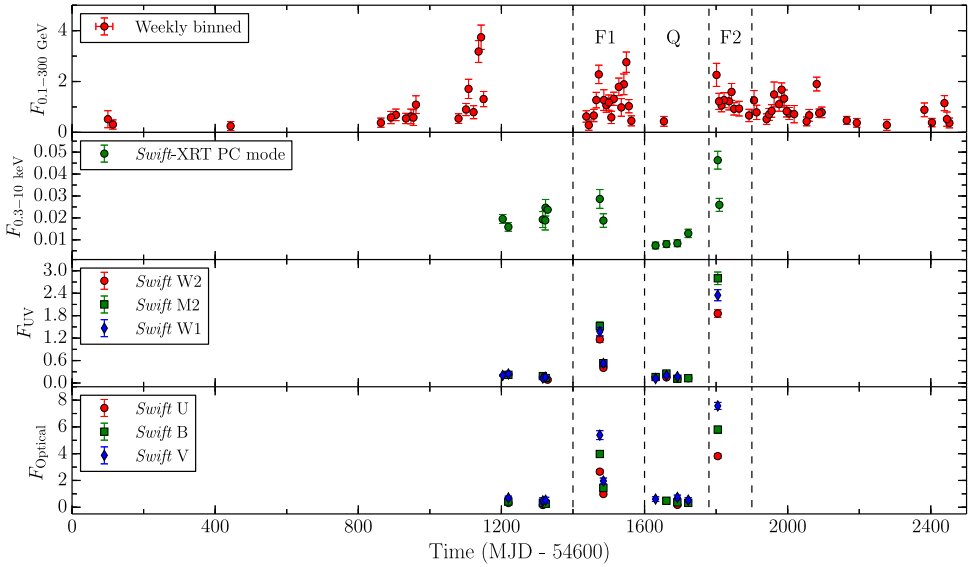

Figure 1. Multi-wavelength light curves of SBS 0846+513 covering the period from 2008 August to 2015 July. Top panel represents the weekly binned γ-ray light curve with flux units of 10^{-7} ph cm^{-2} s^{-1}. The remaining three panels correspond to *Swift* observations binned as one point per observation Id. *Swift*-XRT data points are in units of counts s^{-1} and Swift UVOT observations are in units of 10^{-12} erg cm^{-2} s^{-1}. F1 and F2 are two high-activity periods and Q represents a low-activity state selected for SED modeling. See the text for details.

Table 3
Summary of SED Generation Analysis

Activity State	Period[a]	Flux[b]	*Fermi*-LAT Photon Index[c]	Test Statistic[d]	N_{pred}[e]
F1	56000−56200	9.04 ± 0.61	2.11 ± 0.04	1085.60	1056.01
Q	56200−56380	1.53 ± 0.56	2.56 ± 0.26	17.32	150.97
F2	56380−56500	9.92 ± 0.84	2.10 ± 0.05	732.15	658.01

Activity State	Exp.[f]	Photon Index[g]	*Swift*-XRT Flux[h]	Normalization[i]	Stat.[j]
F1	4.75	1.45 ± 0.28	$1.02^{+0.32}_{-0.21}$	1.15 ± 0.26	81.42/77
Q	19.14	1.61 ± 0.23	$0.39^{+0.10}_{-0.07}$	0.52 ± 0.01	105.14/131
F2	7.63	1.34 ± 0.16	$1.68^{+0.31}_{-0.25}$	1.69 ± 0.23	142.28/177

Activity State	V[k]	B[k]	Swift UVOT U[k]	$W1$[k]	$M2$[k]	$W2$[k]
F1	3.67 ± 0.20	2.71 ± 0.13	1.82 ± 0.09	0.95 ± 0.06	1.02 ± 0.06	0.79 ± 0.04
Q	0.62 ± 0.10	0.39 ± 0.06	0.18 ± 0.06	0.16 ± 0.02	0.16 ± 0.02	0.14 ± 0.01
F2	7.57 ± 0.26	5.81 ± 0.23	3.82 ± 0.18	2.35 ± 0.15	2.80 ± 0.17	1.86 ± 0.10

Notes.
[a] Time interval considered for SED modeling, in MJD.
[b] Integrated γ-ray flux in 0.1−300 GeV energy range in units of 10^{-8} ph cm^{-2} s^{-1}.
[c] Photon index calculated from γ-ray analysis.
[d] Significance of detection using likelihood analysis.
[e] Number of predicted photons during the time period under consideration.
[f] Net exposure in kiloseconds.
[g] Photon index derived from X-ray analysis.
[h] Observed flux in units of 10^{-12} erg cm^{-2} s^{-1}, in 0.3−10 keV energy band.
[i] Normalization at 1 keV in 10^{-4} ph cm^{-2} s^{-1} keV^{-1}.
[j] Statistical parameters: C-stat./dof.
[k] Average flux in *Swift* UVOT bands in units of 10^{-12} erg cm^{-2} s^{-1}.

central black hole following Ghisellini & Tavecchio (2009). The electrons radiate via synchrotron and inverse Compton scattering processes in the presence of a tangled but uniform magnetic field. The synchrotron and synchrotron-self Compton (SSC) radiations are derived from the observer's frame using the prescriptions of Finke et al. (2008). Along with SSC, photons from external components such as the accretion disk, the BLR, and the torus also participate in the IC scattering (e.g., Dermer et al. 2009; Ghisellini & Tavecchio 2009). The jet powers are calculated following Celotti & Ghisellini (2008).

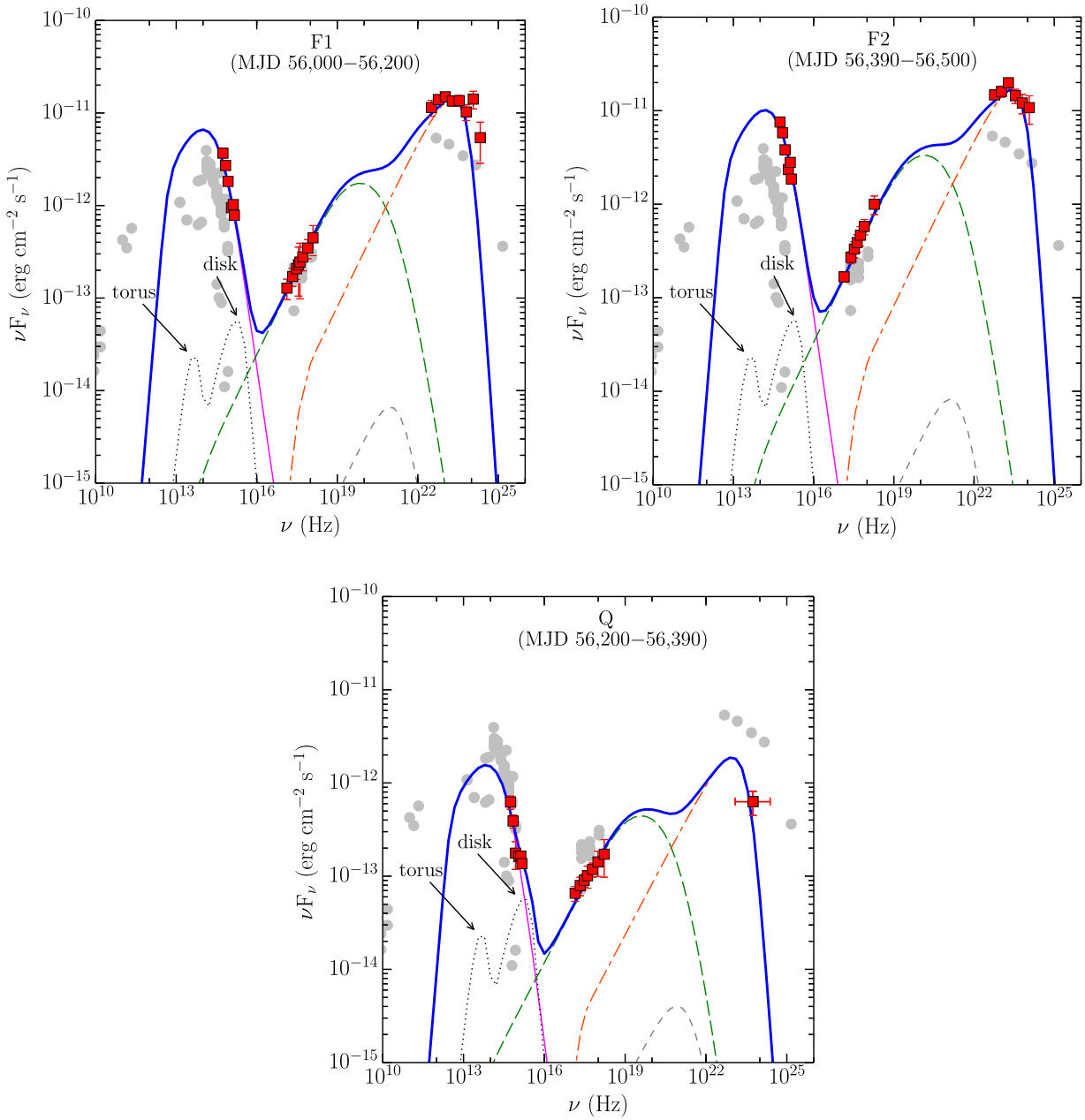

Figure 2. SEDs of SBS 0846+513 during various activity states. The red squares represent the simultaneous observations from *Swift* and *Fermi*-LAT, whereas the gray circles represent the archival observations. Thermal radiations from the accretion disk and the torus are shown by the dotted black line. The pink thin solid, green long dashed, orange dash–dash–dot, and gray dashed lines correspond to synchrotron, SSC, EC-BLR, and EC-torus emissions, respectively. The blue thick solid line is sum of all the radiative components.

Protons are assumed to carry only the inertia of the jet and do not contribute to the observed radiation. Furthermore, it should be noted that based on H_β line parameters, Shen et al. (2011) estimated the black hole mass of SBS 0846+513 as $\sim 9.77 \times 10^7 M_\odot$. The broadband SED of this object does not show any evidence for the presence of the big blue bump (a characteristic signature of the accretion disk emission), so the observed optical spectrum probably has significant contamination from jet emission not taken into account in Shen et al. (2011), and therefore these estimates should be taken with caution. Recently Foschini et al. (2015) have performed a detailed optical spectroscopic analysis of a sample of NLSy1 galaxies, including SBS 0846+513. They used the H_β line luminosity instead of continuum at 5100 Å to derive $M_{\rm BH}$, and thus were able to avoid the flux contamination from the host galaxy and the jet. They found $M_{\rm BH}$ of SBS 0846+513 as $3.2 \times 10^7 M_\odot$. We reproduce the observed optical UV part of the SED with a combination of the accretion disk model and synchrotron emission in such a manner so as not to overproduce the observations. With this we derive a black hole mass as $M_{\rm BH} = 5.5 \times 10^7 M_\odot$ and the disk luminosity as $L_{\rm disk} = 1 \times 10^{44}$ erg s^{-1}. Our $M_{\rm BH}$ estimation via SED modeling agrees within a factor of two to that derived by Foschini et al. (2015) and is therefore reliable.

The modeled SEDs are shown in Figure 2 and the associated modeling parameters are given in Table 4. In Figure 2 the red

Table 4
Summary of the Parameters Used/Derived from the SED Modeling

Parameter	Symbol	*F*1	*Q*	*F*2
Particle spectral index before break energy	p	1.8	1.9	1.8
Particle spectral index after break energy	q	7.0	7.2	7.0
Magnetic field in Gauss	B	3.5	4.2	3.9
Particle energy density in erg cm^{-3}	$U'_{\rm e}$	0.40	0.70	0.42
Bulk Lorentz factor	Γ	13	7	13
Break Lorentz factor of electrons	$\gamma'_{\rm brk}$	1088	1047	1278
Maximum Lorentz factor of electrons	$\gamma'_{\rm max}$	3e4	3e4	3e4
Distance of the emission region in parsec ($R_{\rm Sch}$)	$R_{\rm diss}$	0.011 (2100)	0.009 (1700)	0.011 (2100)
Jet power in electrons in log scale	$P_{\rm e}$	43.87	43.39	43.89
Magnetic jet power in log scale	$P_{\rm B}$	43.95	43.38	44.05
Radiative jet power in log scale	$P_{\rm r}$	44.50	43.81	44.66
Jet power in protons in log scale	$P_{\rm p}$	46.04	45.69	46.05

Note. Viewing angle is assumed as 3° and the characteristic temperature of the dusty torus as 900 K. For a disk luminosity of 1×10^{44} erg s^{-1} and black hole mass of $5.5 \times 10^7\ M_\odot$, the size of the BLR is 0.01 pc (1947 $R_{\rm Sch}$).

squares represent the simultaneous observations from *Swift* and *Fermi*-LAT and gray circles correspond to archival data.[8]

As can be seen in Figure 2, the SED of SBS 0846+513 has a typical double hump structure, similar to blazars. The synchrotron radiation dominates the observed optical UV spectra in all the activity states and the contribution from the accretion disk is negligible. This is supported by the detection of a high optical polarization (>10%) during the 2013 April flare (associated here with F2 state) of SBS 0846+513 (Maune et al. 2014). Also, the observed optical UV spectrum is extremely steep which is difficult to explain by accretion disk model. A high synchrotron emission indicates a high level of SSC emission, which is evident in Figure 2. A flat X-ray spectrum is observed and successfully explained by SSC mechanism. We observed a relatively hard γ-ray spectrum in both the flaring states (see Table 3) which, according to our model, is reproduced by the EC-BLR process. Visual inspection suggests the possible existence of a break in the γ-ray spectrum which we interpret as a consequence of EC-BLR peak to lie within the LAT energy range. From SED modeling of both the flaring periods, we constrain the location of the emission region to be at the outer edge of the BLR where a major contribution of the seed photons for IC scattering is provided by BLR clouds. These results are different from that obtained by D'Ammando et al. (2012, 2013) where the γ-ray emission is explained on the basis of EC-torus mechanism and the location of the emission region was constrained to be far out from the BLR. Since the emission region is located relatively closer in our case, the derived magnetic fields are higher and the size of the emission regions are smaller compared to them. On the other hand, during the low-activity state we found the emission region to be located within the BLR.

3.4. Intranight Optical Variability

We observed SBS 0846+513 on a total of six nights between 2012 November and 2013 March, using the 2 m Himalayan *Chandra* Telescope and the 1.3 m telescope at Devasthal. The differential light curves of the NLSy1 galaxy relative to each of the two comparison stars and the comparison stars themselves are shown in Figure 3. The source is considered as variable only when it shows correlated variations both in time and amplitude relative to the selected pair of comparison stars. To quantify INOV we use two statistical tests, *C* statistics and *F* statistics. The *C* parameter is defined as follows:

$$C = \frac{\sigma_T}{\sigma_{\rm CS}} \tag{2}$$

where σ_T and $\sigma_{\rm CS}$ are the standard deviations of the source and the comparison star differential light curves, respectively. The source is considered to have shown INOV if $C \geqslant 2.576$, which corresponds to 99% confidence level (Jang & Miller 1997). On the other hand, the method of *F* statistics takes into account the ratio of two variances given as

$$F = \frac{\sigma_T^2}{\sigma_{\rm CS}^2} \tag{3}$$

where σ_T^2 is the variance of source-comparison star differential light curves and $\sigma_{\rm CS}^2$ is the variance of the comparison star-star differential light curves. We then compare the derived *F* values with the critical *F* value, F_ν^α, where α is the significance level[9] and ν ($=N_p - 1$) is the degree of freedom for the light curve. We assume the source to be variable only if both the computed *F* values, with respect to the differential light curves of the source to each of the two comparison stars, are greater than the critical *F* value. The results of *F* and *C* statistics are given in Table 5. It should be noted that *C* statistics might be a more appropriate quantity to check for the presence of variability, especially when the comparison star light curves are not steady. Further, we have not found any correlation between the variability pattern of FWHM of the point source with that observed in the source light curves. Therefore, we conclude that the observed INOV are true flux variations of SBS 0846+513. As can be seen in Figure 3 and Table 5, the source has shown significant flux variations on all of the nights. This suggests a duty cycle of 100% using both *C* and *F* statistics. The duty cycle is defined as the ratio of the time over which the object shows flux variations to the total observing time. It is

[8] http://tools.asdc.asi.it/SED/

[9] A significance level of $\alpha = 0.01$ corresponds to a confidence level >99%.

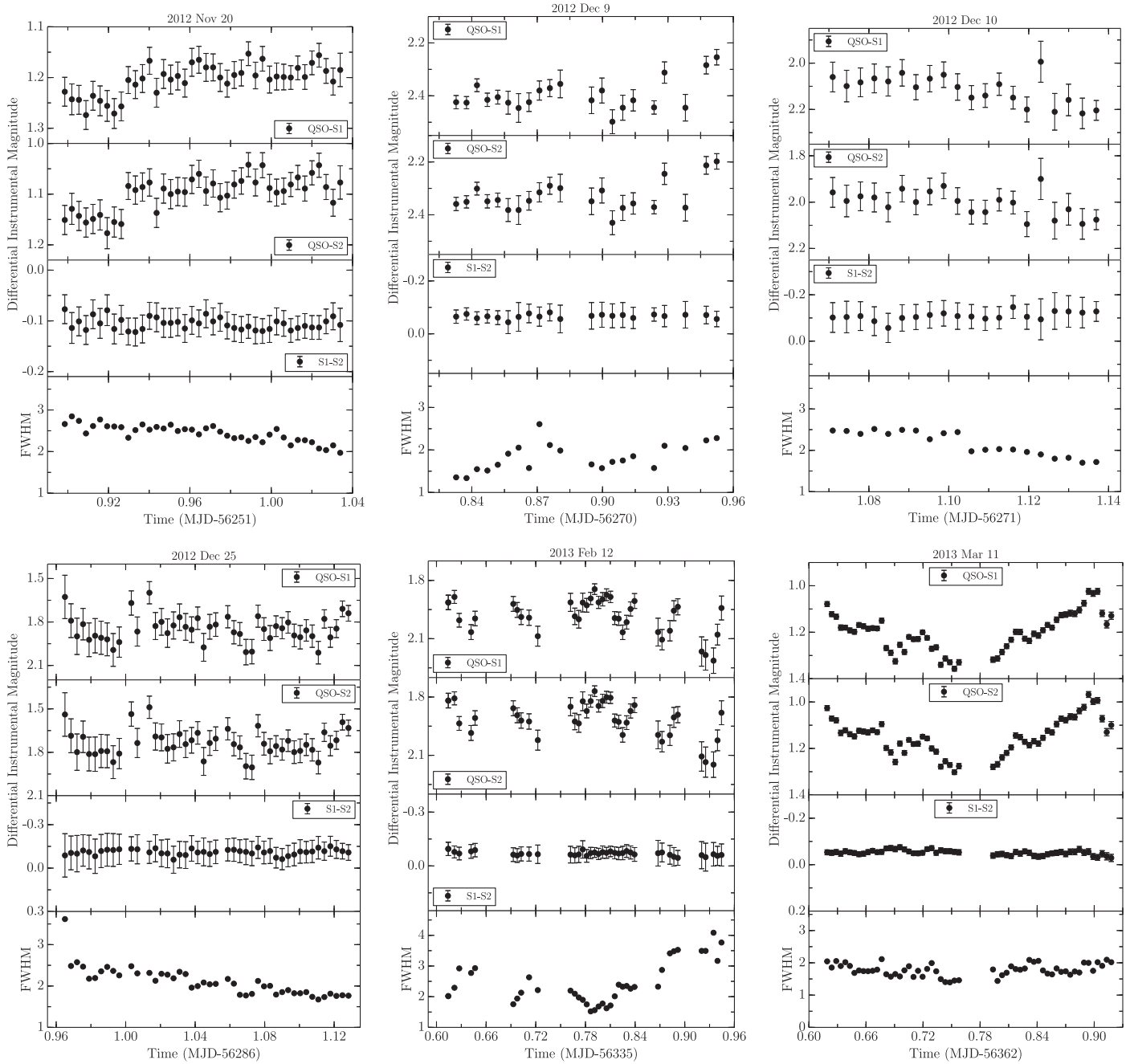

Figure 3. Intranight differential light curves of SBS 0846+513. The bottom panel of each plot shows the variations of the FWHM of the stellar images during the night. QSO refers to the source SBS 0846+513, while S1 and S2 denote the two comparison stars selected to generate the differential light curves.

calculated as follows:

$$DC = 100\frac{\sum_{i=1}^{n} N_i(1/\Delta t_i)}{\sum_{i=1}^{n}(1/\Delta t_i)}\ \%, \quad (4)$$

where $\Delta\, t_i = \Delta t_{i,\mathrm{obs}}(1+z)^{-1}$ is the duration of the monitoring session of a source on the ith night, corrected for the redshift z. $N_i = 1$ if INOV is detected and otherwise 0. Considering the INOV patterns exhibited by other γ-NLSy1 galaxies studied in our earlier work (Paliya et al. 2013a, 2014), the overall duty cycle for γ-NLSy1 galaxies is found to be 55% and 81% according to C and F statistics, respectively. Such high-amplitude (ψ>3%), high-duty cycle (∼70%) INOV are generally seen in the BL Lac objects (e.g., Stalin et al. 2004). This supports the idea that the INOV characteristics of γ-NLSy1 galaxies are similar to blazars.

An interesting phenomenon is the observation of INOV behavior of a source during the γ-ray flaring period. It has been shown by Paliya et al. (2014), based on the results of another γ-NLSy1 galaxy 1 H 0323+342, that the chances of detecting large amplitude INOV are higher during the γ-ray flaring period. Coincidentally, one of the INOV observations reported here (2013 March 11) was taken during one of the γ-ray flares of SBS 0846+513 (period F2). During that night, the brightness of the source first decreased by ∼0.3 mag and then increased by a similar amount within ∼7 hr. (see Figure 3). As

Table 5
Log of INOV Observations of SBS 0846+513

Date yyyy mmm dd	ψ (%)	*C1*	*C2*	Status	*F1*	*F2*	Status
[1]	[2]	[3]	[4]	[5]	[6]	[7]	[8]
2012 Nov 20	11.99	2.62	2.93	V	6.85	8.60	V
2012 Dec 9	24.37	6.98	6.88	V	48.78	47.33	V
2012 Dec 10	22.15	3.32	2.92	V	11.00	8.53	V
2012 Dec 25	41.30	4.55	4.51	V	20.67	20.32	V
2013 Feb 12	36.76	7.56	7.91	V	57.15	62.50	V
2013 Mar 11	33.27	7.91	7.64	V	62.53	58.38	V

Note. Column information is as follows: (1) observation date; (2) INOV amplitude in percent; (3) and (4) *C*-values computed for differential light curves relative to the steadiest pair of comparison stars; (5) variability status according to *C* statistics with V as variable and NV as non-variable; (6) and (7) values of *F* parameter for the differential light curves relative to the two comparison stars; and (8) variability status as per *F* statistics.

can be seen in this plot, on top of the large flare, many small amplitude but fast variations are also visible. Such fast INOV features are also seen in the γ-NLSy1 galaxies 1 H 0323 + 342 and PMN J0948+0022 (Paliya et al. 2013a, 2014). This hints at the existence of high incidence of INOV during γ-ray flaring activity and consequently argues for a jet based origin for the observed INOV.

4. CONCLUSIONS

In this work, we present a multi-wavelength study of the γ-ray emitting NLSy1 galaxy SBS 0846+513. The INOV observations reported here are new and the observation on any particular night spans more than five hours. We summarize our findings below.

1. The multi-wavelength light curves of the source show multiple episodes of γ-ray flaring activities which are also reflected in lower frequency observations. However, the existence of close correlation between γ-ray and X-ray wavelengths could not be statistically confirmed due to the sparseness of the data.
2. A statistically significant curvature is noticed in the seven years averaged LAT spectrum of SBS 0846+513, a feature generally seen in the γ-ray spectra of powerful FSRQs.
3. The broadband SEDs of SBS 0846+513 show the typical double hump structure similar to blazars, with a steep optical and a relatively hard γ-ray spectrum.
4. The modeling of the SEDs with a one-zone leptonic emission model indicates the optical UV spectrum to be dominated by synchrotron emission, whereas the X-ray spectra are well explained by SSC process. The γ-ray regions of the SEDs are explained by IC scattering of BLR photons. It is found that during both the flaring activity states, the emission region was located at the outer edge of the BLR, while during the low-activity state it was well within the BLR.
5. Significant INOV is noticed on all the six nights of ground based optical observations. Interestingly, a large amplitude INOV is seen during the γ-ray flaring period F2.

We thank the referee for constructive comments that helped improve the manuscript. This research made use of the data obtained from HEASARC provided by the NASA's Goddard Space Flight Center. Part of this work is based on archival data, software, or online services provided by the ASI Science Data Center (ASDC). This research has made use of the XRT Data Analysis Software (XRTDAS) developed under the responsibility of the ASDC, Italy. Use of *Hydra* cluster at Indian Institute of Astrophysics is acknowledged.

REFERENCES

Abdo, A. A., Ackermann, M., Ajello, M., et al. 2009, ApJL, 707, L142
Acero, F., Ackermann, M., Ajello, M., et al. 2015, ApJS, 218, 23
Ackermann, M., Ajello, M., Atwood, W. B., et al. 2015, ApJ, 810, 14
Arnaud, K. A. 1996, in ASP Conf. Ser. 101, Astronomical Data Analysis Software and Systems V, ed. G. H. Jacoby, & J. Barnes (San Francisco, CA: ASP), 17
Barthelmy, S. D., Barbier, L. M., Cummings, J. R., et al. 2005, SSRv, 120, 143
Baumgartner, W. H., Tueller, J., Markwardt, C. B., et al. 2013, ApJS, 207, 19
Boller, T., Brandt, W. N., & Fink, H. 1996, A&A, 305, 53
Breeveld, A. A., Landsman, W., Holland, S. T., et al. 2011, in AIP Conf. Ser. 1358, Gamma Ray Bursts, ed. J. E. McEnery, J. L. Racusin, & N. Gehrels (Melville, NY: AIP), 373
Burrows, D. N., Hill, J. E., Nousek, J. A., et al. 2005, SSRv, 120, 165
Cash, W. 1979, ApJ, 228, 939
Celotti, A., & Ghisellini, G. 2008, MNRAS, 385, 283
D'Ammando, F., Orienti, M., Finke, J., et al. 2012, MNRAS, 426, 317
D'Ammando, F., Orienti, M., Finke, J., et al. 2013, MNRAS, 436, 191
Dermer, C. D., Finke, J. D., Krug, H., & Böttcher, M. 2009, ApJ, 692, 32
Doi, A., Nagai, H., Asada, K., et al. 2006, PASJ, 58, 829
Finke, J. D., Dermer, C. D., & Böttcher, M. 2008, ApJ, 686, 181
Foschini, L. 2011, in Proc. Science 126, Narrow-Line Seyfert 1 Galaxies and their Place in the Universe, ed. L. Foschini, M. Colpi, L. Gallo et al. (Trieste: POS)
Foschini, L., Angelakis, E., Fuhrmann, L., et al. 2012, A&A, 548, A106
Foschini, L., Berton, M., Caccianiga, A., et al. 2015, A&A, 575, A13
Foschini, L., Ghisellini, G., Tavecchio, F., Bonnoli, G., & Stamerra, A. 2011, A&A, 530, A77
Gehrels, N., Chincarini, G., Giommi, P., et al. 2004, ApJ, 611, 1005
Ghisellini, G., & Tavecchio, F. 2009, MNRAS, 397, 985
Goodrich, R. W. 1989, ApJ, 342, 224
Grupe, D., & Mathur, S. 2004, ApJL, 606, L41
Itoh, R., Tanaka, Y. T., Akitaya, H., et al. 2014, PASJ, 66, 108
Itoh, R., Tanaka, Y. T., Fukazawa, Y., et al. 2013, ApJL, 775, L26
Jang, M., & Miller, H. R. 1997, AJ, 114, 565
Jiang, N., Zhou, H.-Y., Ho, L. C., et al. 2012, ApJL, 759, L31
Kalberla, P. M. W., Burton, W. B., Hartmann, D., et al. 2005, A&A, 440, 775
Komossa, S., Voges, W., Xu, D., et al. 2006, AJ, 132, 531
Liu, H., Wang, J., Mao, Y., & Wei, J. 2010, ApJL, 715, L113
Maune, J. D., Eggen, J. R., Miller, H. R., et al. 2014, ApJ, 794, 93
Monet, D. G., Levine, S. E., Canzian, B., et al. 2003, AJ, 125, 984
Osterbrock, D. E., & Pogge, R. W. 1985, ApJ, 297, 166
Paliya, V. S., Sahayanathan, S., Parker, M. L., et al. 2014, ApJ, 789, 143
Paliya, V. S., Stalin, C. S., Kumar, B., et al. 2013a, MNRAS, 428, 2450
Paliya, V. S., Stalin, C. S., & Ravikumar, C. D. 2015, AJ, 149, 41
Paliya, V. S., Stalin, C. S., Shukla, A., & Sahayanathan, S. 2013b, ApJ, 768, 52
Pounds, K. A., Done, C., & Osborne, J. P. 1995, MNRAS, 277, L5
Roming, P. W. A., Kennedy, T. E., Mason, K. O., et al. 2005, SSRv, 120, 95
Schlafly, E. F., & Finkbeiner, D. P. 2011, ApJ, 737, 103
Shakura, N. I., & Sunyaev, R. A. 1973, A&A, 24, 337
Shen, Y., Richards, G. T., Strauss, M. A., et al. 2011, ApJS, 194, 45
Stalin, C. S., Krishna, Gopal., Sagar, R., & Wiita, P. J. 2004, JApA, 25, 1
Tavecchio, F., & Ghisellini, G. 2008, MNRAS, 386, 945
Xu, D., Komossa, S., Zhou, H., et al. 2012, AJ, 143, 83
Yao, S., Yuan, W., Zhou, H., et al. 2015, MNRAS, 454, L16
Zhou, H.-Y., Wang, T.-G., Dong, X.-B., Li, C., & Zhang, X.-G. 2005, ChJAA, 5, 41